Sequence Sensitivity in Membrane Remodeling by Polyampholyte Condensates

Sayantan Mondal[†] and Qiang Cui[*,†,‡,¶]

†*Department of Chemistry, Boston University, 590 Commonwealth Avenue, Boston, MA 02215, United States*

‡*Department of Physics, Boston University, 590 Commonwealth Avenue, Boston, MA 02215, United States*

¶*Department of Biomedical Engineering, Boston University, 44 Cummington Mall, Boston, MA 02215, United States*

E-mail: qiangcui@bu.edu, Tel:(+1)-617-353-6189

Abstract

Intrinsically disordered peptides (IDPs) have been found to undergo liquid-liquid phase separation (LLPS) and produce complex coacervates that play numerous regulatory roles in the cell. Recent experimental studies have discovered that LLPS at or near the membrane surface helps in the biomolecular organization during signaling events and can significantly alter the membrane morphology. However, the molecular mechanism and microscopic details of such processes still remain unclear. Here we study the effect of polyampholyte and polyelectrolyte condensation on two different anionic membranes, as they represent a majority of naturally occurring IDPs. The polyampholytes are fifty-residue polymers, made of glutamate(E) and lysine(K) with different charge patterns. The polyelectrolytes are separate chains of E_{25} and K_{25}. We first calibrate the MARTINI v3.0 forcefield and then perform long-timescale coarse-grained molecular dynamics simulations. We find that condensates formed by all the polyampholytes get adsorbed on the membrane. However, the strong polyampholytes (i.e., blocky sequences) can remodel the membranes more prominently than the weaker ones (i.e., scrambled sequences). Condensates formed by the blocky sequences induce a significant negative curvature ($\sim 0.1\ nm^{-1}$) and local demixing of lipids, whereas those by the scrambled sequences tend to wet the membrane to a greater extent without generating significant curvature or demixing. We perform several microscopic analyses to characterize the nature of the interaction between membranes and these condensates. Our analyses of interaction energetics reveal that membrane remodeling and/or wetting are favored by enhanced interactions between polyampholytes with lipids and the counterions.

Introduction

Liquid-liquid phase separation (LLPS) is a phenomenon that has been widely studied in recent years due to its importance in various biological processes.[1–4] Intrinsically disordered proteins (IDPs) and nucleic acids have emerged as key regulators of LLPS in biological systems, due to the presence of multivalent interactions.[5–7] LLPS is related to intracellular compartmentalization through the formation of membraneless organelles (e.g., nucleoli, P-bodies, stress granules, Cajal bodies, etc.) that support various cellular functions including stress response, protein degradation, signal transduction, and therefore also implicated in diseases.[8–10] In the last decade, there has been a growing interest in understanding the formation, structure, and dynamics of such macromolecular condensates in the bulk phase, both theoretically and experimentally.[11–15]

Recent studies have suggested that LLPS at the lipid membrane is biologically important.[16–20] It was also observed that LLPS at the membrane surface can induce significant curvatures, local demixing, lipid ordering, vesicle biogenesis, and tubulation.[21–29] Therefore, LLPS near the membrane surface can serve as a novel mechanism for membrane remodeling in cells, in addition to the much discussed mechanisms such as hydrophobic insertion, scaffolding, protein crowding, and coating.[30–32] Despite the importance and interest in general, only a few theoretical investigations have been directed toward understanding the mechanism of LLPS-induced large-scale structural transformations of a lipid bilayer or vesicle, from a molecular perspective.

It has been shown that the single-chain properties of an IDP are well correlated with the phase behavior.[33–38] The conformational ensemble of IDPs can be altered by the presence of a membrane. Hence, this could be manifested in the phase behavior of the condensates formed by these IDPs. For example, it has been recently observed that non-specific interactions between fused in sarcoma low-complexity domain (FUS-LCD) and lipids can strongly modulate IDP condensation and single-chain behavior.[39] Phosphatidylserine membranes prefer β-sheet structures of FUS, whereas phosphatidylglycerol membranes promote unstructured conden-

sates. In such instances, the membrane might cause changes in the IDP phase behavior that are difficult to predict based solely on the increased local protein concentration caused by membrane adsorption.[16] Specific interactions between membrane and proteins help control the location and timing of LLPS for specific cellular functions (e.g., signaling).[40] On the other hand, LLPS helps concentrate specific protein components for regulating the efficiency and sensitivity of signaling events.[19,20] Moreover, phase behaviors of the peripheral proteins and the lipid membrane can be coupled.[41,42] In a lattice model-based study, it was found that membranes close to the critical point can promote protein phase separation on its surface, even in conditions where LLPS is not feasible in the bulk.[43] Nevertheless, using a similar approach, we recently further demonstrated that the critical behavior of the membrane is not required to promote the pre-wetting transition.[44] To rationalize the experimentally observed membrane bending and tubulation following the adsorption of an IDP condensate,[22,27] continuum mechanics-based models were used. However, it is difficult to comprehend the molecular details of the underlying driving force using such models alone.

Here, the systems of interest are condensates formed by polyelectrolytes and polyampholytes in the presence of model anionic lipid bilayers. Our interest in such systems is driven by the observation that many naturally occurring IDPs contain long stretches as well as scrambled sequences of charged amino acids. Approximately 75% natural IDPs are polyampholytes as demonstrated by a BLAST search of the UniProtKB database.[45] The polyelectrolytes and polyampholytes can readily undergo LLPS, even in low concentrations, often referred to as coacervation.[46–50] These coacervates find a wide range of applicability that comprise of coatings, adhesives, food preservation, rheology controllers, tissue engineering, agriculture, and biomedicine.[46,51–60] Coacervates are also used to build synthetic analogs of living cells (protocells) owing to their crowded interior, unique core-shell property, and molecular sequestration capability.[61,62] Given its wide range of uses, it is evident that these charged IDPs are present in animal cells that can undergo LLPS and interact with the cell membrane. There exist a number of studies on the phase behavior of polyampholytes and

polyelectrolytes in the bulk solution phase.[14,50,63–67] Recently, we unraveled the membrane remodeling ability of polyelectrolytes (namely, E_{30} and K_{30}).[21] We showed that polyelectrolytes coacervates can induce significant negative curvature and local lipid segregation in anionic lipids. Another recent model simulation study used dissipative particle dynamics to show that LLPS of disordered proteins with two domains can induce membrane bending and lateral separation (i.e., demixing) of lipids.[68] However, the same for polyampholytes (and the sensitivity towards its sequence), which seems to have more relevance to the natural IDPs, has hitherto remained unexplored.

An extension of the celebrated Flory-Huggins (FH) formalism[69,70] for polyelectrolytes and polyampholytes was achieved by Overbeek and Voorn.[71] For a mixture of polycations and polyanions of the same length (N) and equal (but opposite) charges, the mean-field free energy per lattice site ($\mathcal{F}$) is given by Eq. (1),

$$\beta\mathcal{F} = (\phi/N)ln(\phi/2) + (1-\phi)ln(1-\phi) - \alpha(\sigma\phi)^{3/2}, \tag{1}$$

where ϕ is the total volume fraction of the polymers, the parameter α is determined by charge per site, σ is the linear charge density, and $\beta = (k_BT)^{-1}$. When σ^3N exceeds a value of 0.5 (critical point), the polyelectrolyte solution phase separates into polymer-rich and polymer-deficient regions that is known as complex coacervation. More recently, a combination of the FH theory with a random phase approximation (RPA) was used to study binodal and spinodal phase behaviors of neutral polyampholytes.[72] Nevertheless, minimalistic mean-field models cannot capture sequence dependence or even multivalent interactions, which are shown to be important factors in understanding LLPS of IDPs.[66] Hence, molecular simulations and more sophisticated models are needed to investigate the molecular details associated with complex coacervation.

To extract long timescale structural changes, the sampling of their vast conformational ensemble becomes computationally expensive in atomic resolution. Hence, one often resorts

to either coarse-graining approaches[35,64,73–75] or numerical solutions of field theory-based equations.[14,72] However, the development of CG models as well as their calibration against experimental results (often unavailable) for IDPs become hard to achieve. Different levels of coarse-grained (CG) approaches have been applied to study LLPS, for example, with multiple beads per residue,[76–78] single-bead per residue,[35,75,79] and even multiple-residues per bead.[80,81] However, the transferability of these forcefields remains a critical issue. Lindorff-Larsen and co-workers have shown that by increasing the attractive interaction (by $\sim 10\%$) between protein and water beads in MARTINI v3.0, one can improve the single-chain conformational behavior of several natural IDPs.[82] Hummer and co-workers observed good agreement with experiments by re-balancing the protein-protein non-bonded interaction parameters using MARTINI v2.2 for LLPS of FUS-LCD and a DNA-binding protein TDP-43.[83,84]

Specifically for EK-polyampholytes, Das and Pappu investigated the sequence-ensemble relationship with implicit solvent atomistic simulations by using ABSINTH forcefield.[45] They showed that a segregated sequence (e.g., $E_{25}K_{25}$) is more prone to form hairpin-like conformations compared to a well-mixed sequence (e.g., $(EK)_{25}$). The latter explores conformations that are similar to Flory random coils. The differing conformational dynamics of single-chains are manifested in the phase diagram of these polyampholytes, as studied by several groups.[14,36,65] It was established, by field-theoretic simulations and random phase approximation (RPA) based phase diagrams that polyampholytes with scrambled charge patterns have a narrower 'two-phase region' compared to sequences with a blocky charge pattern. De Pablo and co-workers, again with RPA-based calculations, demonstrated that the presence of charge blocks within a random sequence facilitates the formation of denser and more salt-resistant coacervates.[65] Their study also supports the increased width of the two-phase region as observed by Shea and co-workers. More recently, Marrink and co-workers used MARTINI v3.0.[76] based CG simulations to study the phase behaviors of E_{30} and K_{30} at several salt concentrations.[64] Encouragingly, the simulations captured the key trend observed in the experimental studies of Priftis and Tirrell, who analyzed the sensitivity of ionic strength

on complex coacervation of E_{30} and K_{30} mixtures.[63]

The MARTINI forcefield is capable of providing a satisfactory description of the lipid bilayers.[85,86] In addition, the favorable MARTINI results for natural IDPs[82–84] and E/K-polyelectrolytes,[64] encouraged us to use MARTINI v3.0 to study the interaction of polyelectrolytes, and several polyampholytes with model lipid membranes as representative examples of biomolecular condensate/membrane interactions.[18] Here, we ask the following questions: (i) How does the sequence (or, the charge patterns) of the E/K-polyampholytes affect the extent of membrane remodeling by the condensates? (ii) How does a membrane modulate the structure of the condensates depending on the sequence of its constituent polyampholytes? (iii) What are the driving factors for these mutual structural alterations? In the subsequent sections, we aim to answer these questions with several long-timescale (tens of μs for each system) CGMD simulations, from structural, energetic, and kinetic viewpoints. These simulations provide the first microscopic analysis of the sequence sensitivity of condensate-membrane interactions and the subsequent effect on their morphology. The study shall lay the groundwork for future investigation of physical factors that govern protein LLPS at the membrane surface involving more complex proteins and lipid membranes.[17,40,42]

Methods

The polyampholytes and polyelectrolytes have been modeled with the explicit-solvent CG MARTINI (v3.0) force-field.[76] The atomistic models have been created with `pymol`[87] followed by a conversion into the CG model with `martinize2` script. We first aim to calibrate the single chain behavior of polyampholytes with respect to the earlier published results of Das and Pappu.[45] To this goal, we have followed the method demonstrated by Lindorff-Larsen and co-workers,[82] by systematically increasing the protein-water interactions. In this description, each E and K residue is modeled by two and three CG beads, respectively (one backbone and one/two side-chain beads). The side-chain bead of each E contains -1e charge and the second

side-chain bead of each K contains $+1e$ charge. In addition to this, the N- and C-termini, respectively, contain $+1e$ and -1e charges.

For the membranes, we have chosen two different anionic membranes made of different ratios of palmitoyl oleoyl phosphatidylcholine (POPC, zwitterionic) and palmitoyl oleoyl phosphatidylglycerol (POPG, anionic). The two different ratios are: (i) POPC:POPG=50:50 and (ii) POPC:POPG=70:30. Although the percentage of anionic lipids might seem higher than those of physiologically relevant ones ($\sim 10\% - 15\%$), local concentrations on a large membrane patch or a giant vesicle can be much higher due to spatial heterogeneity in membrane composition. In our previous study, we showed that more that 20% POPG content is required to observe stable membrane adsorption of polyelectrolytes.[21] For the kinetic studies, we have used membranes with asymmetric leaflets, where only one of the two leaflets contains anionic lipids. This has been done to direct the polyampholytes adsorption only on one surface in the PBC setup.

For the single chain simulations we have used a 15 nm^3 cubic box and for the bulk LLPS/coacervation study we have randomly inserted 50 polyampholytes (or, 50 polyelectrolytes of each type) in a 30 nm^3 cubic box filled with MARTINI CG water beads. These systems contain Na^+ and Cl^- ions with a concentration of 15 mM. We have simulated the single chain systems for 20 μs and the bulk LLPS systems for 10 μs. After the formation of the condensate in the bulk phase, we have extracted the coordinates of the coacervate with its hydration and ionic environment up to 1 nm. Then, the condensate have been placed near an already equilibrated and tensionless lipid bilayer. All the systems are then energy minimized by using the steepest-descent algorithm followed by equilibration in the isothermal-isobaric (NPT) ensemble for 2 μs which allows the coacervate to form stable contacts with the bilayer. After that, 5 μs production runs are carried out in an NPT ensemble with a 200 ps trajectory dumping rate. All the equilibration simulations are propagated with a time step of 10 fs and production simulations are propagated with a time step of 20 fs, using the leap-frog algorithm. We have used the V-rescale thermostat[88] ($\tau_T = 1\ ps^{-1}$) at 298

K and Parrinello-Rahman barostat[89] with semi-isotropic pressure coupling ($\tau_P = 12\ ps^{-1}$) at 1 bar to make the bilayer tensionless. For initial equilibration purposes, we have used Berendsen barostat[90] with τ_P=6 ps^{-1}. The electrostatic interactions are screened with a reaction field (ϵ_r) of 15 within a cut-off of 1.1 nm and vdW interactions are also terminated at 1.1 nm with the Verlet cut-off scheme. The simulations are carried out with the GROMACS 2018.3 package[91] and analyses are performed with a combination of Fortran90 codes, `gmx tools`, and plumed 2.5.3.[92] For visualization purposes, we have used VMD 1.9.3.[93]

Results and discussion

Single chain behavior

The polyampholyte chains are of the same molecular weight and charge content but only differ in the permutation of the E and K residues. Das and Pappu defined a parameter, κ to differentiate these polymers from one another.[45] To calculate κ one partitions the sequence into a certain number of overlapping 'blobs' of segment size g (taken to be 5 and 6) and calculate the charge asymmetry (σ_i) according to Eq. (2).

$$\sigma_i = \frac{(f_+ - f_-)_i^2}{(f_+ + f_-)_i} \tag{2}$$

where f_+ and f_- are the fractions of positive and negative charges respectively, in the i^{th} blob. Following this, κ is calculated by normalizing the mean square deviation of σ_i (indicated as δ) for a particular sequence by the maximum possible value of δ (by considering all the sequences). κ can take up values between 0 and 1, with $\kappa = 0$ denoting the most scrambled and $\kappa = 1$ denoting the most segregated sequence. Later, Sawle and Ghosh defined another parameter called sequence charge decoration or 'SCD' defined as follows [Eq.3][94]

$$SCD = \frac{1}{N}\left[\sum_{m=2}^{N}\sum_{n=1}^{m-1} q_m q_n (m-n)^{\frac{1}{2}}\right], \tag{3}$$

where N is the chain length, 'q' denotes the charges, and m and n are the indices. Therefore, in this formalism, a more segregated/blocky charge pattern would exhibit a higher and negative value of SCD.

In our study, we have used the nomenclature used by Das and Pappu (that is, sv1, sv2 ... sv30 etc.). Out of several sequences studied before, here we choose five representative sequences that cover a broad spectrum of κ and SCD values [Table 1]. Note that, the single chain radius of gyrations (R_g) increases monotonically with SCD but not with κ. We find that all the polyampholytes exhibit predominantly a collapsed conformation with the original MARTINI v3.0 force field parameters. Therefore, we rescale the protein-water interactions and find that a 15% upscaling can make the single chain properties, such as the radius of gyration [Table 1] and end-to-end distance profiles [Figure 1], well-behaved according to the reference data.[45] The average end-to-end distance profiles ($\langle R_{ij} \rangle$) are described in the following way. For a certain value of $|i-j| = k$, $\langle R_{ij} \rangle$ is defined as

$$\langle R_{ij}(k) \rangle = \frac{1}{N-k} \sum_{n=1}^{N-k} (\vec{r}_{n+k} - \vec{r}_n), \tag{4}$$

where N is the total number of beads, i and j are the bead indices, and $\vec{r}$ is the position vector. A monotonically increasing $\langle R_{ij} \rangle$ with respect to $|i-j|$ indicates a random-chain like behavior whereas, the emergence of non-monotonicity is associated with the preference for 'bent' structures.

However, we observe that sequences with (very) low κ values (that is, a high degree of charge scrambling) such as '$(EK)_{25}$', do not behave well, even with the rescaled version of MARTINI v3.0. Hence, due to the non-transferability of force field parameters and the relatively narrower phase separation window, we do not include such sequences in the present study. Nonetheless, we performed some analyses to address the origin of the discrepancy, later in this paper.

We additionally look into the distribution of the end-to-end distances of the polymers while they are isolated in water, and compare that with the conformational ensemble in the

Table 1: The single chain sequences and their radius of gyration values obtained with the original MARTINI v3.0 and its 'scaled' version along with the respective κ and SCD values. λ is the parameter that indicates the extent of 'scaling' with $\lambda = 1.00$ being the original 'unscaled' forcefield. It is observed that a 15% scaling of the protein-water interactions can produce R_g values that are close to the reference.

	Single chain R_g in Å			Parameters	
Sequence	$\lambda = 1.00$	λ= 1.15	Ref.[45]	κ	SCD
sv13	14.3 ± 0.86	21.9 ± 0.40	24.1	0.095	-2.98
sv21	14.5 ± 0.41	20.9 ± 0.35	22.4	0.274	-4.06
sv24	13.0 ± 0.55	17.7 ± 1.13	17.5	0.445	-17.03
sv27	13.2 ± 0.35	19.1 ± 0.56	19.5	0.673	-11.4
sv30	12.9 ± 0.52	16.6 ± 0.24	16.8	1.000	-27.9

sv13 = KEKKKEKEKKEKKKEEEKKKEEEKEKKKEEKKEKKEKKEEEEEEEKEEKE
sv21 = EEEEEEEEEKEKKKKKEKEEKKKKKKEKKEKKKKEKKEEEEEEKEEEKKK
sv24 = EEEEKEEEEEKEEEEEEEEEEEEKKKEEKKKKKEKKKKKKKEKKKKKKKK
sv27 = KKEKKKEKKEEEEEEEEEEEEEEEEEEEEKEEKKKKKKKKKKKKKKKKEKK
sv30 = EEEEEEEEEEEEEEEEEEEEEEEEKKKKKKKKKKKKKKKKKKKKKKKKKK

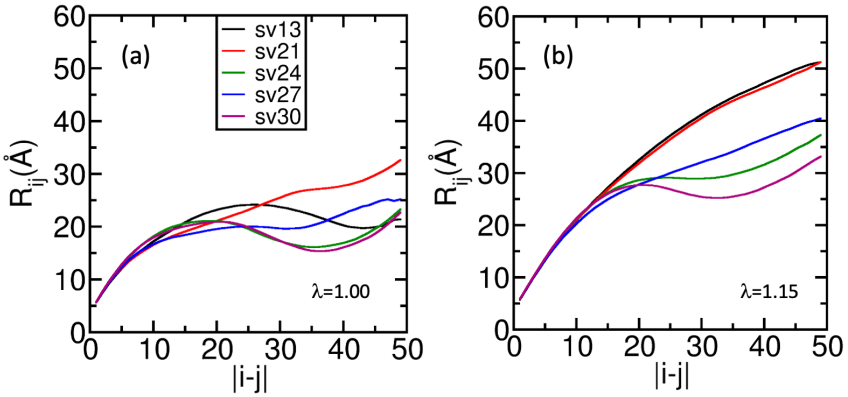

Figure 1: End-to-end distance profiles (R_{ij}) for the five chosen sequences with (a) the original MARTINI v3.0 forcefield and (b) the 'scaled' MARTINI v3.0 forcefield, where i and j are the residue indices. The original MARTINI v3.0 produces collapsed conformations even for the low κ polymers. With $\lambda = 1.15$, MARTINI v3.0 produces the correct trend in R_{ij}, that is, non-monotonic increase (indicates a 'bent' or 'hairpin-like' conformation) for high κ sequences and Flory random coil-like structure for the low κ sequences.

membrane-adsorbed condensates [Figure 2]. It is observed that the conformational ensemble is weakly dependent on the presence of anionic lipid membranes for the polyelectrolytes [Figure 2(a) and 2(b)] and polyampholytes with lower κ values [Figure 2(c) and 2(d)]. On the other hand, for the sequences with a high κ value, the polyampholytes become more extended

in the presence of a membrane [Figure 2(e), 2(f), and 2(g)].

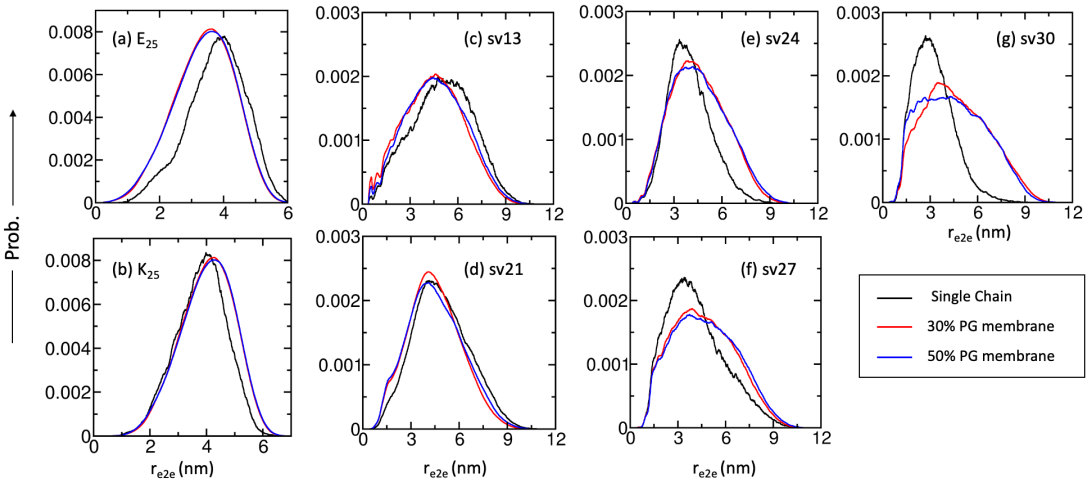

Figure 2: The end-to-end distance distributions for polyelectrolytes and polyampholytes in isolated and membrane-condensate systems: (a) E_{25}, (b) K_{25}, (c) sv13, (d) sv21, (e) sv24, (f) sv27, and (g) sv30. The polyampholytes with a higher κ value becomes more extended in the presence of a membrane.

Shape of the coacervate upon membrane adsorption

When randomly placed in the bulk (i.e., without membranes), the polyelectrolytes and all the variants of polyampholytes underwent LLPS to form complex coacervates which are close to spherical in shape. With an increasing degree of charge scrambling (i.e., decreasing κ) the coacervates deviate from a spherical shape and also become less compact. In the presence of anionic membranes, the coacervates exhibit spontaneous adsorption. We find that coacervates formed by different polyampholytes spread differently on the membranes. It is observed that coacervates formed by polyampholytes with a high κ value tend to wet the membrane surface less compared to those with a lower κ value. This is also influenced by the effective attraction of the membrane.

Evidently, there is a competition between the inter-polymeric interaction strength and the polymer-membrane adhesion strength. For example, coacervates formed by sv21 and sv13 completely lose their spherical (bulk) shape after being adsorbed on 50% POPG membrane,

whereas coacervates of polyelectrolytes (E_{25} and K_{25}) and sv30 are able to hold their shape after getting adsorbed. The other two sequences, namely sv27 and sv24 show an intermediate degree of wetting. With a 30% POPG membrane, the coacervates exhibit comparatively less wetting due to the lower effective attraction of the membrane. To quantify the spreading of the polyampholytes droplets we calculate the radius of gyration (R_g) of the droplets in water (bulk) as well as in the membrane adsorbed state [Table 2]. The respective snapshots from simulations are provided in Figure 3.

Table 2: Time averaged radius of gyration (R_g) of the coacervates in their bulk phase and membrane adsorbed state. In the bulk, the coacervates are seen to become less compact with increasing charge scrambling. A similar trend is observed in their membrane adsorbed state. The low κ coacervates are more spread out compared to the high κ ones.

	R_g of the coacervate (nm)		
Polymers	Bulk	50% PG	30% PG
E_{25} + K_{25}	5.54 ± 0.16	6.83 ± 0.04	5.98 ± 0.06
sv30	5.64 ± 0.05	7.02 ± 0.08	6.02 ± 0.07
sv27	5.75 ± 0.17	9.29 ± 0.44	6.60 ± 0.27
sv24	5.82 ± 0.09	9.05 ± 0.52	7.25 ± 0.29
sv21	6.23 ± 0.35	12.46 ± 0.75	9.47 ± 0.61
sv13	6.35 ± 0.39	12.17 ± 0.78	11.79 ± 0.98

Lipid demixing

Multicomponent lipid membranes are complex structures composed of a variety of lipid species that differ in their headgroup chemistry, acyl chain length, saturation, and packing density. Such lipid bilayers can exhibit local heterogeneity that can get enhanced due to the presence of adsorbed polymers, bound proteins, or other macromolecules.[95–98] This can result in the formation of lipid domains, which can have different physical properties than the surrounding membrane. Local lipid demixing can eventually lead to an altered membrane morphology (due to different spontaneous curvatures of lipid components), which has far-reaching consequences in biology.

Here we observe local demixing due to the adsorption of the coacervates on the membrane.

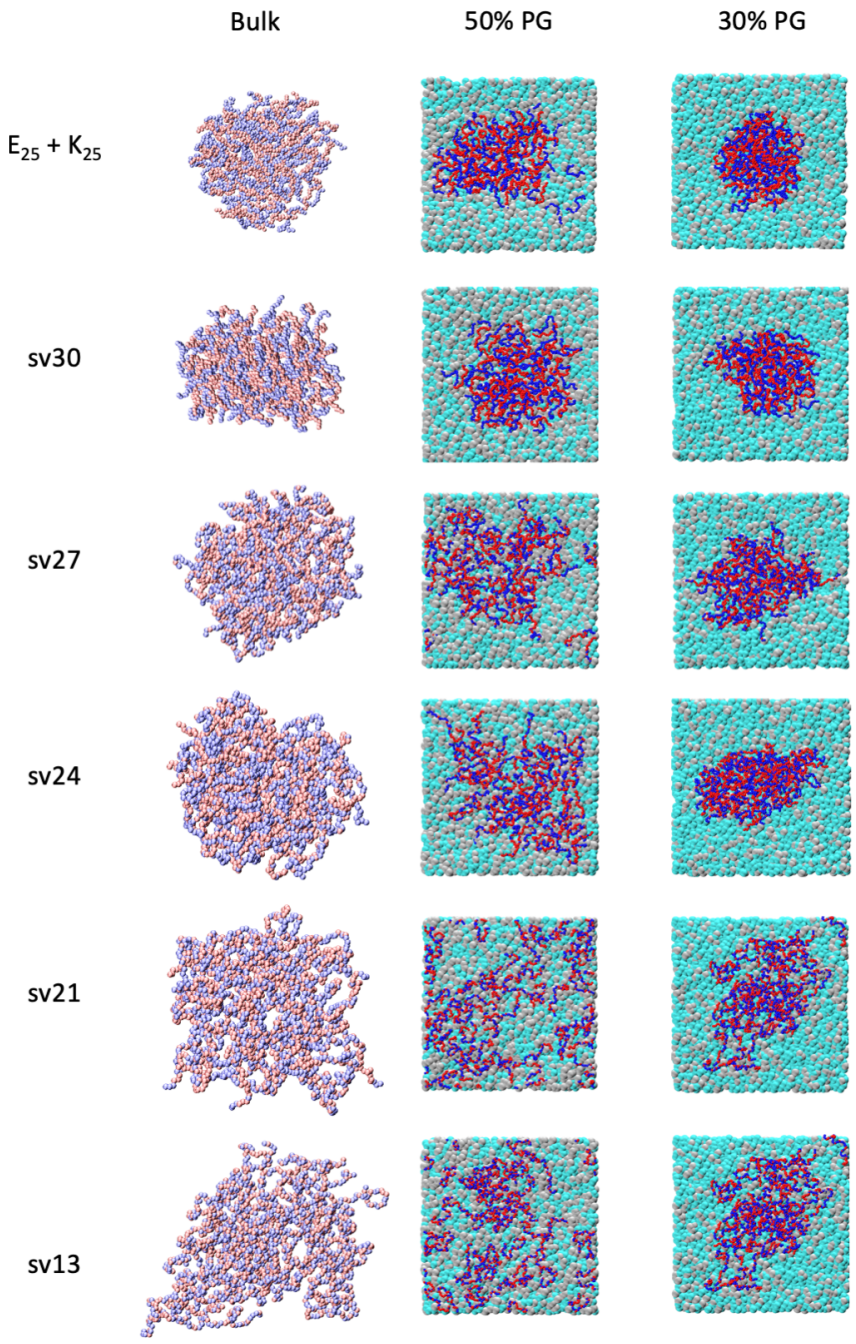

Figure 3: Snapshots of the condensates and their membrane adsorbed state for polyelectrolytes and polyampholytes with different degree of charge blockiness. In the bulk, low κ polyampholytes form less compact and more porous condensates. The condensates formed by polyampholytes with a higher degree of charge scrambling tend to spread and wet the membrane surface more. Here, the Lysine, Glutamate, POPC, and POPG residues are shown in blue, red, cyan, and grey, respectively.

Without the coacervates, the long-timescale membrane-only systems with POPC and POPG do not show any phase separation with MARTINI 3 parameters. To quantify, we compute the grid-wise and time-averaged charge density (as given by Eq. 5) of lipid head groups by constructing a 30×30 grid in the XY plane along the bilayer [Figure 4],

$$\sigma_{ij} = \langle n^{POPG} \rangle_{ij} \times (-1). \tag{5}$$

Here, i and j are the grid indices, σ is the time-averaged charge density, and $\langle n^{POPG} \rangle$ is the time-averaged number of POPG heads in that particular grid. We find a significant degree of local demixing in the upper leaflet (in contact with the coacervate) for the polyelectrolytes and polyampholytes with blocky sequences (i.e., high κ values). On the other hand, the weaker polyampholytes could not induce a significant local demixing of the POPG molecules.

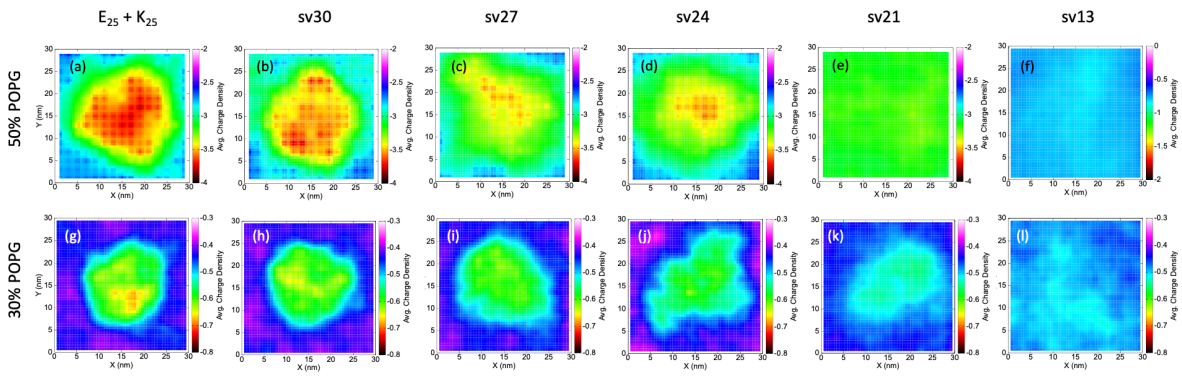

Figure 4: Local de-mixing of lipids at the upper leaflet induced by the adsorption of the coacervates. The time-averaged grid-wise charge density is plotted as a projection in the XY plane. It is observed that the coacervates of strong polyampholytes (high κ) can induce more significant local demixing compared to the coacervates formed by the weak polyampholytes (low κ). [Note that the color bar scales are different for 50% POPG and 30% POPG systems, to visualize the spatially resolved charge density profiles distinctly.]

Demixing is entropically unfavourable. Therefore, there must exist an enthalpic component that overcompensates for the entropy loss. An earlier theoretical study by Ben-Shaul *et al.* can be recapitulated to understand the above phenomena.[95] By employing a mean-

field description of a charged sphere adsorbing to a charged surface, they showed that the entropic penalty can be overcome through optimal charge matching. In a membrane, in addition to the counterion redistribution, the lipid molecules can laterally diffuse to facilitate the optimal charge matching between the membrane and the coacervate. As the interior of the coacervate is dynamic, a simultaneous spatial redistribution also takes place within the coacervate to concentrate the positively charged Lys residues near the demixed negatively charged POPG headgroups. This eventually drives local demixing.

The consequences of lipid demixing in multicomponent lipid membranes can be significant. For example, the formation of lipid domains can affect the diffusion and mobility of membrane-associated proteins, leading to changes in membrane signaling and cellular function. Additionally, lipid domains can act as sites for the recruitment of specific proteins or lipids, leading to the formation of specialized microdomains within the membrane.

Curvature generation

Lipid membranes are dynamic structures that are capable of generating and responding to changes in curvature. The generation of curvature in lipid membranes is a fundamental process that is essential to a diverse range of cellular functions such as membrane scission, fusion, cargo trafficking, motility, organelle shaping *etc.*[99] Through the generation of curvature, cell membranes can adopt different morphologies and respond to internal/external mechanical stress. There exist various mechanisms by which a lipid membrane can develop curvature, as discussed below.

Membrane curvatures could arise because of the shapes of the constituent lipid molecules, lipid phase separation, membrane tension, or, due to the interaction with proteins/polymers.[100–106] For example, lipids with bulky headgroups, such as phosphatidylserine (PS) and phosphatidylethanolamine (PE), tend to form highly curved regions of the membrane due to steric hindrance and electrostatic repulsion between headgroups. However, POPC and POPG exhibit no spontaneous curvature due to their fairly cylindrical shapes.[107] In the membrane-only

systems, the bilayers do not show any persistent spontaneous curvature and phase-separation under the same simulation conditions. The membrane is also made tensionless by applying a semi-isotropic pressure coupling. Therefore, it is clear that the generated curvature is induced by the adsorption of the coacervate on the membranes.

Curvature generation due to membrane-protein interactions can be further divided into two broad classes of mechanisms: (i) hydrophobic insertion,[30,108] and (ii) coating/crowding of proteins.[109] In the case of curvature generation by hydrophobic insertion, the inserted peptide residues alter the area of one of the membrane leaflets which leads to mechanical stress and steric repulsions.[30,108,110] In our systems of interest, the polymers are highly charged and avoid the hydrophobic interior of the membrane. On the other hand, curvature generation through coating/crowding occurs when proteins aggregate along the membrane surface, but without insertion. Such crowding and scaffolding generate steric pressure that drives the membrane deformation and leads to a positive curvature,[111] and the mechanism is particularly relevant to IDPs clustered at membrane surfaces.[111,112] However, the sign of the resulting curvature and morphology might depend on the chain flexibility and strength of adsorption.[104,113]

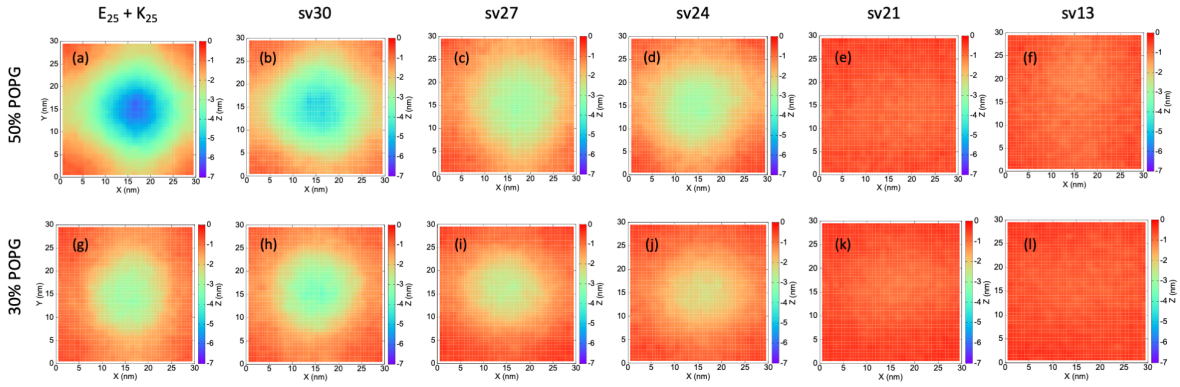

Figure 5: Generation of negative curvature (reflected by the time-averaged membrane Z-surface) by polyelectrolytes and polyampholytes condensates on two different anionic membranes. Weak polyampholytes with a low κ value is mostly spread over the membrane and cannot generate a significant curvature. Strong polyampholytes with a high κ value can generate more prominent negative curvatures in the order of 0.1 nm^{-1}.

We observe that coacervates formed by polyelectrolytes and strong polyampholytes (with

Table 3: Estimation of the generated negative curvature by the coacervates formed by polyelectrolytes and strong polyampholytes. These values are the result of a numerical fit of the time-averaged Z-surfaces plotted in Figure 5.

	Curvature (nm^{-1})	
Polymers	50% PG	30% PG
E_{25} + K_{25}	0.120	0.102
sv30	0.095	0.085
sv27	0.083	0.082
sv24	0.090	0.079

high κ values) induce a prominent negative curvature at and around the region of contact. As the weaker polyampholytes tend to wet the membrane surface and cannot hold their spherical shape, they cannot induce any curvature. In Figure 5, we plot the time-averaged Z-surface (normal to the membrane) of the bilayer-coacervate systems by translating the whole system with respect to the center of mass of the coacervate to the center of the box at each time step. The whole XY-surface is divided into 30×30 grids and the time-averaged Z-coordinate for each grid is calculated.

Kim and Sung performed a theoretical analysis to understand the sign of the membrane curvature upon the adsorption of polymers of different nature.[104] According to their study, a weakly bound flexible polymer can produce a positive curvature whereas a strongly bound flexible polymer results in a negative curvature. The latter is observed in our simulations. They estimated the order of magnitude of the curvature (C) by Eq. (6) as follows,

$$C \sim -\left(\frac{k_B T \varepsilon}{\kappa b}\right) \delta, \tag{6}$$

Here T is the temperature, κ denotes the membrane bending modulus, ε is the polymer adsorption strength, b is the polymer attraction range, and δ is related to the thickness (ξ) of the adsorbed polymer layer as $\xi = b(1 + \delta)$. Some typical values (also used by Kim and Sung) are as follows: $b \sim 1\ nm$, $\kappa \sim 10\ k_B T$,[86] $\delta \sim 0.1$, and $\varepsilon \sim (T_c/T) \sim 10$. With these approximate numerical values, Eq. (6) yields $C \sim 0.1\ nm^{-1}$. The estimated mean curvatures for our systems also fall in the range of $0.08 - 0.12\ nm^{-1}$, which corroborates well with the

theoretical prediction (Table 3).

Contact pair analysis

Here, we report the the total number of time-averaged contacts between different pairs, after reaching equilibrium, according to Eq. (7),

$$q_{ij}(t) = \frac{1 - [r_{ij}(t)/r_0]^6}{1 - [r_{ij}(t)/r_0]^{12}}, \tag{7}$$

where $q_{ij}(t)$ is a measure of contact between i^{th} and j^{th} beads at a given time t, $r_{ij}(t)$ is the distance between i^{th} and j^{th} beads at time t, and $r_0 = 5$ Å . The particular choice of the contact order parameter (Eq. 7) has been made in order to make it smoothly vary from 1 to 0, rather than the usual Heaviside function. Therefore, the time-averaged total number of contacts (Q) is described by Eq. (8), where τ is the number of time steps over which the average is taken

$$Q = \frac{1}{\tau} \sum_t Q(t) = \frac{1}{\tau} \sum_{ij,t} q_{ij}(t). \tag{8}$$

In Figure 6, we plot Q for polyampholyte-polyampholyte (P-P) and polyampholyte-lipid (P-L) pairs in their bulk as well as bilayer adsorbed state, against the parameter κ. We find that Q_{P-P} increases with κ which indicates that the coacervate remains more compact for stronger polyampholytes, even in the presence of a membrane. For any given κ, it can be seen that the P-P contacts get depleted [Figure 6(a)] in their membrane adsorbed states. Interestingly, for sv27 the decrease in Q_{P-P} from its respective bulk value is more that the other sequence variants. Q_{P-L}, on the other hand, shows a non-monotonic behavior on 50% POPG membrane but a monotonic increase on 30% POPG, with respect to κ. The depletion of P-P contacts and increment in the P-L contacts get manifested in the interaction energetics as described in the subsequent section.

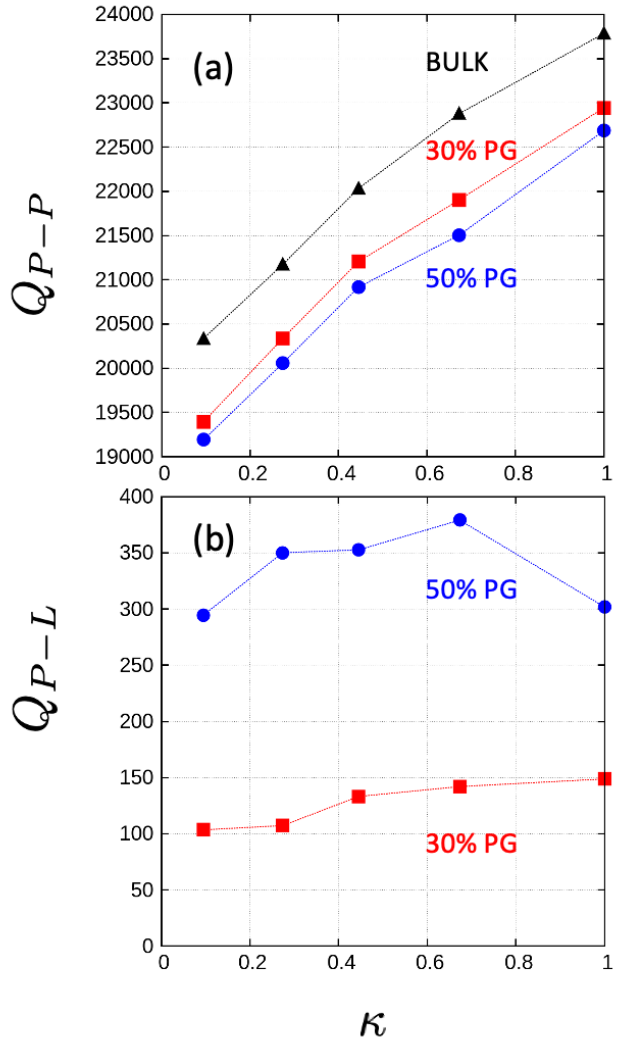

Figure 6: Number of contacts between (a) polyampholytes (Q_{P-P}) in the bulk coacervate (black), 30% POPG membrane (red), and 50% POPG membrane; (b) polyampholytes -lipid (Q_{P-L}) for 30% (red) and 50% (blue) POPG membranes. For a given value of κ, Q_{P-P} is lower in the membrane adsorbed state compared to the bulk coacervate. [The dotted lines are drawn to guide the eyes and are not constructed of actual data points].

Energetics

Here we aim to understand the driving force for the adsorption of the coacervate, wetting of the membrane surface, and the other subsequent events. We compute the component-wise average pair interaction energies (the sum of Lennard-Jones and Coulomb interactions). Out of 21 distinct pairs, we only plot the significant contributions in Figure 7 for two different

anionic membranes with respect to the charge blockiness parameter, κ.

In Figure 7 we plot the scaled interaction energy (ΔE) divided by the total number of polyampholytes (N_{pol}). ΔE is scaled by subtracting the interaction energies in the respective bulk coacervate system. For all the systems, we find that the inter-polyampholyte interactions (P-P) get destabilized. To balance this, there are two major stabilizing effects that arise from the polyampholytes-lipid (P-L) and polyampholytes-ion (P-Ion) interactions. In addition to that, the polyampholytes-water (P-W) interactions are also (weakly) stabilizing. For systems with 50% POPG, the individual stabilizing effects of P-L and P-I surpass the destabilizing effect from depleting P-P pair [Figure 7(a)]. Interestingly, for systems with 30% POPG, the stabilization obtained through the increase in the P-L interactions is solely not enough to compensate for the destabilizing effect that enters through the P-P interaction energies [Figure 7(b)]. Here, P-I and P-W attractive interactions play a major role in driving the bilayer wetting. The extent of both destabilization and stabilization amplifies with increasing κ. Further decomposition of the interaction energies for different sub-ensembles reveals that E-E and K-K interactions become stabilized, but E-K interactions become more destabilized at the same time. The decomposition of the P-L pair interactions reveals that the E-POPG interactions are destabilizing whereas, the K-POPG interactions provide a huge stabilizing effect. An earlier study by Stachowiak and co-workers hypothesized that the increased overlap among the IDP residues was the driving force of negative membrane curvature generation, primarily based on a continuum mechanics framework.[22] However, we rather observed the opposite for both polyelectrolytes and polyampholytes coacervate adsorption on membranes.

Here we have focused solely on interaction energies, while it was suggested that entropic factors associated with counter-ion release is a major driving force for bulk coacervation.[67] Here, we have not analyzed the entropic component in detail, since coarse-grained models may not be able to capture the proper entropic components of the relevant free energies.[114] For example, a previous study on the hydrophobic association of helical peptides[115] revealed

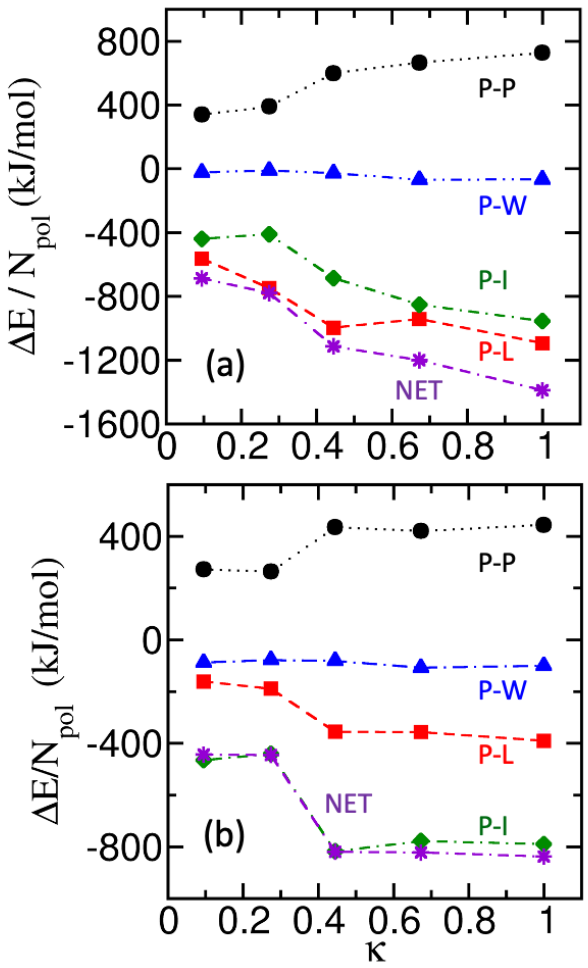

Figure 7: Interplay between different pair interaction energies plotted against κ for: (a) 50% POPG membrane and (b) 30% POPG membrane. $\Delta E = \langle E \rangle - E_{bulk}$, is the scaled interaction energy per polyampholyte. A positive value of ΔE denotes destabilizing effect whereas a negative value of ΔE denotes stabilizing interactions. The reported values are block averaged by dividing the trajectory into blocks of 100 ns. Error bars are either one or two orders of magnitude smaller, and hence not shown for a clearer representation. [Notations: P=polyampholytes, L=lipids, I=ions, and W=water.]

that the MARTINI (previous to v3.0) could not capture an entropy-driven dimerization unless the CG water model features a quadrupole moment comparable to that of atomistic water clusters.[74] Interestingly, in our previous study, we showed that MARTINI v3.0 can capture the enthalpy-entropy balance relatively well, in the context of polyelectrolyte association, by comparing it with an atomistic forcefield.[21] In the same paper, it was also shown that MARTINI v3.0 can predict the right trend in the increase or decrease in interaction

energetics among different sub-ensembles. Nevertheless, systematic elucidation of entropic contributions in LLPS and LLPS-membrane interaction requires additional analysis using different CG or potentially atomistic models.[116–118]

Effect of an extra 'bond'

The two coacervates, one formed by E_{25} & K_{25} and ano ther formed by $sv30$, have only one difference at the single chain level. In $sv30$, the E_{25} & K_{25} segments are connected by a harmonic bond. Here we explore the changes observed in their behaviour in the bulk as well as with membranes, solely due to this extra 'bond'. In Table 3 and Figure 5 we have already noted that the generated negative curvatures are higher for E_{25} & K_{25} coacervate than those generated by $sv30$ coacervate. We also showed a greater extent of demixing induced by the E_{25} & K_{25} coacervate (Figure 4). In Figure 8, we provide bar plots to highlight the differences in terms of interaction energies between different pairs.

Figure 8 shows that the magnitude of stabilization/destabilization is higher for E_{25} & K_{25} coacervate than those due to $sv30$ coacervate. Therefore, the membrane remodeling (and subsequent stabilization) abilities of the coacervate get partly reduced due to an extra backbone connection. The 'bond' alters both the enthalpic and entropic contributions of the coacervate-membrane interaction. The entropy of an ideal polymer chain is given by $S = k_B ln[\Omega(\vec{R})]$, where $\vec{R}$ is the end-to-end distance of the polymer chain. The entropy scales as R^2/Nl^2, where N is the number of bonds in the polymer and l is the Kuhn length. From Figure 2 we have noted that the single chain end-to-end distance distribution for $sv30$ becomes wider when the coacervate is adsorbed to the membranes. However, for E_{25} and K_{25}, the distributions of the membrane adsorbed state are markedly similar to those in the bulk. Therefore, from an entropic perspective, the adsorption of $sv30$ is favourable. On the other hand, there is an enthalpic penalty for $sv30$ associated with the spatial reorganization of the coacervate. This is due to the fact that the positively charged K_{25} segment necessarily brings the connected negatively charged E_{25} segment when establishing contacts with the

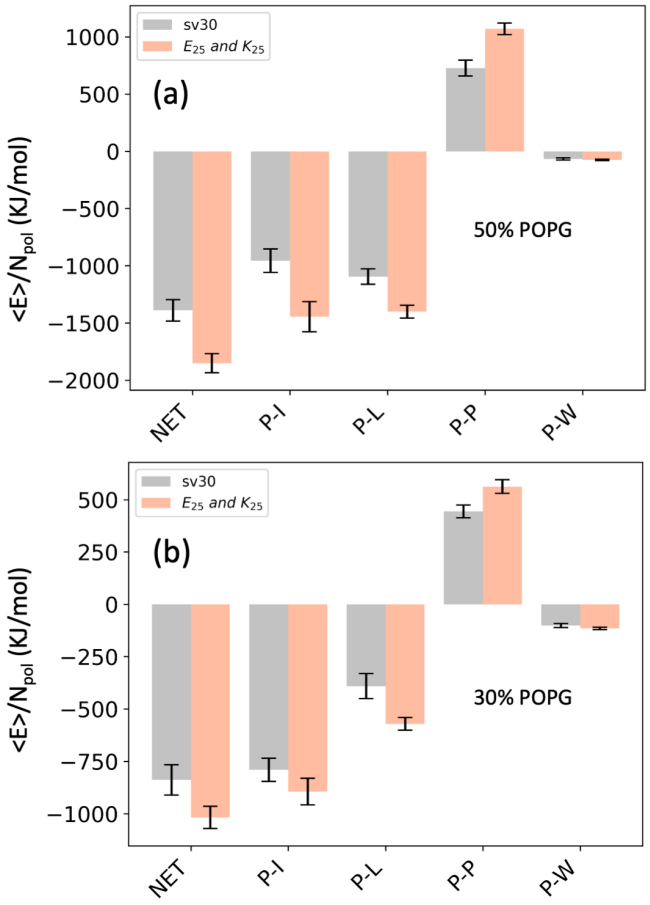

Figure 8: Comparison of the pair interaction energetics upon membrane adsorption of $E_{25} - K_{25}$ and $sv30$. (a) for 50% POPG bilayer and (b) for 30% POPG bilayer. The X- and Y-axes labels bear the same meaning as Figure 7.

negatively charged POPG headgroups of the de-mixed bilayer. This constraint is not present in the 'disconnected' polymers, which are able to maximize enthalpic interactions with the membrane.

Kinetic aspect: Condensation vs. membrane adsorption

The results and observations discussed so far have been inferred from simulations that are carried out by assimilating a pre-equilibrated membrane patch and a pre-formed condensate. This was done to quickly achieve the membrane-adsorbed equilibrium state. However, to answer the question: *What is the sequence of events?*, we have performed additional simulations

starting with randomly distributed polymers around a membrane patch.

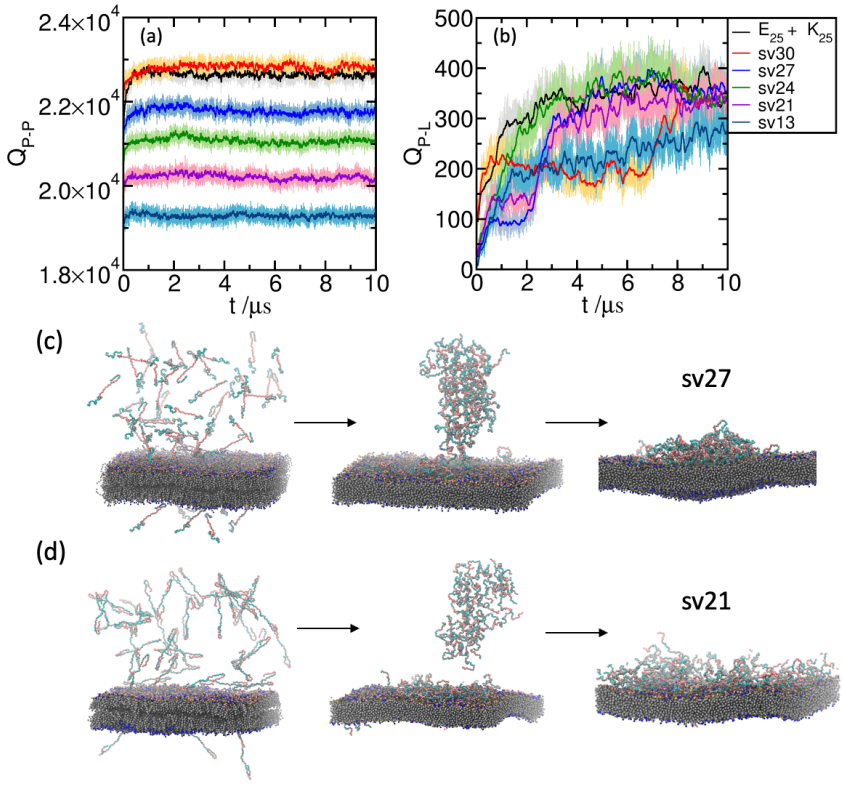

Figure 9: The time-evolution of (a) polymer-polymer (Q_{P-P}) and (b) polymer-lipid (Q_{P-L}) contacts for different systems starting from a randomly distributed polymer configuration. Q_{P-P} shows a fast increase followed by stabilization whereas the growth of Q_{P-L} is slower. The darker traces are obtained by time-averaging. Snapshots of the condensation and membrane adsorption processes for two representative polyampholytes-membrane systems (c) sv27 (high κ) and (d) sv21 (low κ).

The time evolution of different pair contacts is monitored throughout the trajectory according to Eqs. (7) and (8). In Figures 9(a) and 9(b), we respectively plot Q_{P-P} and Q_{P-L} against time. For all the systems polyampholytes condensation precedes membrane adsorption. More than one sequence, namely, sv30, sv27, and sv21 exhibit two jumps in the Q_{P-L} vs *time* plot. This indicates fractional adsorption in the beginning, followed by total adsorption and spread. In Figures 9(c) and 9(d), we provide several representative snapshots to visualize the polyampholyte condensation and membrane adsorption processes. It is also observed that the generation of negative curvature and lipid demixing occur almost simultaneously. During these processes, the coacervate also redistributes its constituent

polyampholytes so that maximum enthalpic stabilization can be achieved. Therefore, the sequence of events is; the formation of the condensate away from the membrane and/or partial adsorption of the polyampholytes on the membrane surface $\rightarrow$ adsorption of the total condensate on the membrane surface $\rightarrow$ generation of negative curvature, segregation of lipids, spatial redistribution of the polyampholytes, and membrane wetting.

Low κ sequences

As mentioned in section 3.1, the polyampholytes-sequences with a low κ value (typically < 0.1) remains collapsed (compared to the reference data[45]) even with a high degree of enhancement in the protein-water interaction (up to 50%). To find out the origin of the discrepancy, we perform several simulations involving two model short-chains, namely $E_{10}K_{10}$ ($\kappa = 1$) and $(EK)_{10}(\kappa = 0)$. With each chain we carry out three simulations: (i) Atomistic MD with CHARMM36m and TIP3P water, (ii) Explicit water MARTINI-3 simulations, and (iii) Bundled-TIP3P atomistic MD simulations with CHARMM36m. The bundling approach, where 4 atomistic water molecules are tetrahedrally bound to each other, was used earlier in several studies to explicitly probe the effect of large MARTINI water beads by keeping everything else in the atomistic resolution.[119,120]

We calibrated the bundled-TIP3P model by adjusting the repulsive potential (C_{12}) to match the desired atomistic density. We further compared (and matched) the position of the peaks and minima in the radial distribution function for MARTINI-3 water and bundled-TIP3P. Therefore, one can huristically accept the bundled-TIP3P as a fine-grained representation of the MARTINI-3 water. Our analyses reveal that for the $\kappa = 0$ chain, the distributions of the R_g and $end - to - end$ distances in the bundled-TIP3P system match that from the MARTINI-3 simulation. However, both of them deviate from the distributions obtained from the pure atomistic system. Nonetheless, for the $\kappa = 1$ chain, distributions from all systems possess a significant overlap. Therefore, it can be concluded that the size of the water bead might restrict the low κ chains to explore certain conformations that are

otherwise present in an atomistic system. Resolution of this problem might involve further calibration of MARTINI-3 for polyampholytes. The results for this section are provided in the **Supporting Information**.

Conclusions

The interaction between phase-separated IDPs with cell membranes has emerged as an important area of research in biophysics. In this paper, we have used CGMD simulations (with MARTINI v3.0) to unravel the sequence sensitivity of polyampholytes in the context of coacervate-membrane interaction followed by the mutual alteration of structures. In a previous study, by using a similar methodology, we showed that polyelectrolytes mixtures (E_{30} and K_{30}) can remodel the membrane by inducing negative curvature and lateral demixing of lipids.[21] We found that the magnitude of bending and demixing depend on the fraction of anionic lipids. Here we have explored the same for polyampholytes with different charge patterns that serve as model systems for a diverse range of naturally occurring IDP sequences. However, we note that the natural IDPs are abundant in low κ polyampholytes, typically less than 0.3.[45]

The rationale behind the choice of MARTINI v3.0 for our systems of interest is partly driven by the work of Marrink *et al.*,[64] who captured the salt concentration dependence of polyelectrolytes in the bulk phase with MARTINI v3.0.[63] Additionally, in the context of EK-polyampholytes a systematic tuning of MARTINI v3.0[82] (by increasing the protein-water LJ interaction strength by 15%) captured the single chain conformational ensemble relatively well. As the single-chain properties are well-correlated with its phase behavior,[33–38] one can assume that 'scaled-MARTINI v3.0' provides a reasonable description of our systems of interest. Nevertheless, the scaled-MARTINI v3.0 fails to capture the correct conformational ensemble for polyampholytes with very low κ or SCD value (well-mixed charge sequences). Our conjecture towards the resolution of this puzzle refers to the representation of water in

MARTINI where one water bead is equivalent to four atomistic water molecules. We showed by employing bundled-water simulations that the size of water can control the single-chain conformations. It could be possible that water at the molecular level plays an important role in directing the conformational dynamics of the low κ sequences, as suggested in several earlier studies in the context of polymer dynamics.[120] Note that, here we use the results of Das and Pappu[45] as a reference which is also from simulations (in implicit solvent and with atomistic resolution). A dearth of experimental data for single-chain properties of polyampholytes (such as SAXS or PRE) makes it difficult to calibrate the force field.

Here we report several interesting aspects of polyampholytes condensate-membrane interactions and their sensitivity to the charge patterning. The key observations are:

1. Polyelectrolytes and polyampholytes with long stretches of similar charges form more compact coacervates. Polyampholyte condensates with segregated single-chain charge patterns (i.e., blocky charge sequences with a high κ) can bend anionic lipid membranes more prominently than those with scrambled charge patterns (associated with a low κ). The extent of lipid demixing also amplifies with increasing blockiness of the sequences.

2. The change in the coacervate shape after getting adsorbed on a membrane depends on the charge patterning. Polyampholytes with a segregated charge pattern tend to partially hold the coacervate shape, whereas those with a scrambled charge pattern tend to wet the membrane by spreading out.

3. Our microscopic component-wise analyses reveal that the inter-polymeric contacts (as well as interaction energies) get depleted upon membrane adsorption which is compensated by the favorable polymer-lipid and polymer-ion interactions. The magnitude of both destabilization and stabilization amplifies with increasing κ. The entropic contribution is not analyzed here, owing to the general difficulty for CG models to capture the entropy-enthalpy balance.[114,115] However, we previously showed that MARTINI v3.0 (without any parameter tuning) can qualitatively capture the relative balance

between entropy and enthalpy.[21]

4. Kinetic studies reveal that condensation away from the membrane precedes membrane adsorption. The findings are consistent with two anionic membranes with different POPG contents.

To conclude, our present study demonstrates that the membrane remodeling ability of coacervates of polyampholytes composed of glutamates and lysines is dependent on its sequence, even if the net charge content is the same. The membrane remodeling ability increases with κ. The observed curvatures ($\sim$0.08-0.12 nm^{-1}) seem relevant to realistic processes such as vesicle biogenesis.[99,121] The present study provides a critical understanding on coacervate-membrane interaction which could be helpful in designing IDPs for specific purposes. Our broader goal is to incorporate more complex (and biologically relevant) proteins and membranes in this framework of study in the future.

Conflicts of interest

The authors declare no conflicts of interest.

Acknowledgement

We thank Prof. Arun Yethiraj for insightful discussions on polyampholytes, especially for the potential impact of water bundling on polyampholyte conformational properties. This work was supported in part by grant NSF-CHE-2154804 to QC. Computational resources from the Extreme Science and Engineering Discovery Environment(XSEDE),[122] which is supported by NSF Grant ACI-1548562, are greatly appreciated; part of the computational work was performed on the Shared Computing Cluster which is administered by Boston University's Research Computing Services (URL: www.bu.edu/tech/support/research/)..

Supporting Information Available

The **Supporting Information** contains results for bundled-TIP3P simulation with $E_{10}K_{10}$ and $(EK)_{10}$; and their comparison with CHARMM36m and MARTINI-3 systems.

References

(1) Hyman, A. A.; Weber, C. A.; Jülicher, F. Liquid-liquid phase separation in biology. *Annu. Rev. Cell Dev. Biol.* **2014**, *30*, 39–58.

(2) Banani, S. F.; Lee, H. O.; Hyman, A. A.; Rosen, M. K. Biomolecular condensates: organizers of cellular biochemistry. *Nat. Rev. Mol. Cell. Biol.* **2017**, *18*, 285–298.

(3) André, A. A.; Spruijt, E. Liquid–liquid phase separation in crowded environments. *Intl. J. Molec. Sci.* **2020**, *21*, 5908.

(4) Posey, A. E.; Holehouse, A. S.; Pappu, R. V. Phase separation of intrinsically disordered proteins. *Meth. Enzymol.* **2018**, *611*, 1–30.

(5) Weng, J.; Wang, W. Dynamic multivalent interactions of intrinsically disordered proteins. *Curr. Opin. Str. Biol.* **2020**, *62*, 9–13.

(6) Zheng, W.; Dignon, G. L.; Jovic, N.; Xu, X.; Regy, R. M.; Fawzi, N. L.; Kim, Y. C.; Best, R. B.; Mittal, J. Molecular details of protein condensates probed by microsecond long atomistic simulations. *J. Phys. Chem. B* **2020**, *124*, 11671–11679.

(7) Corbet, G. A.; Burke, J. M.; Parker, R. Nucleic acid–protein condensates in innate immune signaling. *EMBO J.* **2022**, e111870.

(8) Fefilova, A. S.; Antifeeva, I. A.; Gavrilova, A. A.; Turoverov, K. K.; Kuznetsova, I. M.; Fonin, A. V. Reorganization of Cell Compartmentalization Induced by Stress. *Biomolecules* **2022**, *12*, 1441.

(9) Alberti, S.; Dormann, D. Liquid–liquid phase separation in disease. *Annu. Rev. Genet.* **2019**, *53*, 171–194.

(10) Molliex, A.; Temirov, J.; Lee, J.; Coughlin, M.; Kanagaraj, A. P.; Kim, H. J.; Mittag, T.; Taylor, J. P. Phase separation by low complexity domains promotes stress granule assembly and drives pathological fibrillization. *Cell* **2015**, *163*, 123–133.

(11) Pak, C. W.; Kosno, M.; Holehouse, A. S.; Padrick, S. B.; Mittal, A.; Ali, R.; Yunus, A. A.; Liu, D. R.; Pappu, R. V.; Rosen, M. K. Sequence determinants of intracellular phase separation by complex coacervation of a disordered protein. *Molec. Cell* **2016**, *63*, 72–85.

(12) Abyzov, A.; Blackledge, M.; Zweckstetter, M. Conformational dynamics of intrinsically disordered proteins regulate biomolecular condensate chemistry. *Chem. Rev.* **2022**, *122*, 6719–6748.

(13) Kaur, T.; Raju, M.; Alshareedah, I.; Davis, R. B.; Potoyan, D. A.; Banerjee, P. R. Sequence-encoded and composition-dependent protein-RNA interactions control multiphasic condensate morphologies. *Nat. Comm.* **2021**, *12*, 872.

(14) McCarty, J.; Delaney, K. T.; Danielsen, S. P.; Fredrickson, G. H.; Shea, J.-E. Complete phase diagram for liquid–liquid phase separation of intrinsically disordered proteins. *J. Phys. Chem. Lett.* **2019**, *10*, 1644–1652.

(15) Dinic, J.; Marciel, A. B.; Tirrell, M. V. Polyampholyte physics: Liquid–liquid phase separation and biological condensates. *Curr. Opin. Colloid Interface Sci.* **2021**, *54*, 101457.

(16) Banjade, S.; Rosen, M. K. Phase transitions of multivalent proteins can promote clustering of membrane receptors. *eLife* **2014**, *3*, e04123.

(17) Case, L. B.; Ditlev, J. A.; Rosen, M. K. Regulation of Transmembrane Signaling by Phase Separation. *Annu. Rev. Biophys.* **2019**, *48*, 465–494.

(18) Kusumaatmaja, H.; May, A. I.; Knorr, R. L. Intracellular wetting mediates contacts between liquid compartments and membrane-bound organelles. *J. Cell Biol.* **2021**, *220*, e202103175.

(19) Huang, W. Y. C.; Alvarez, S.; Kondo, Y.; Lee, Y. K.; Chung, J. K.; Lam, H. Y. M.; Biswas, K. H.; Kuriyan, J.; Groves, J. T. A molecular assembly phase transition and kinetic proofreading modulate Ras activation by SOS. *Science* **2019**, *363*, 1098–1103.

(20) Case, L. B.; Zhang, X.; Ditlev, J. A.; Rosen, M. K. Stoichiometry controls activity of phase-separated clusters of actin signaling proteins. *Science* **2019**, *363*, 1093–1097.

(21) Mondal, S.; Cui, Q. Coacervation of poly-electrolytes in the presence of lipid bilayers: mutual alteration of structure and morphology. *Chem. Sci.* **2022**, *13*, 7933–7946.

(22) Yuan, F.; Alimohamadi, H.; Bakka, B.; Trementozzi, A. N.; Day, K. J.; Fawzi, N. L.; Rangamani, P.; Stachowiak, J. C. Membrane bending by protein phase separation. *Proc. Natl. Acad. Sci. USA* **2021**, *118*, e2017435118.

(23) Mangiarotti, A.; Chen, N.; Zhao, Z.; Lipowsky, R.; Dimova, R. Membrane wetting, molding and reticulation by protein condensates. *bioRxiv* **2022**, 2022–06.

(24) Day, K. J.; Kago, G.; Wang, L.; Richter, J. B.; Hayden, C. C.; Lafer, E. M.; Stachowiak, J. C. Liquid-like protein interactions catalyse assembly of endocytic vesicles. *Nat. Cell Biol.* **2021**, *23*, 366–376.

(25) Bergeron-Sandoval, L.-P.; Kumar, S.; Heris, H. K.; Chang, C. L. A.; Cornell, C. E.; Keller, S. L.; Francois, P.; Hendricks, A. G.; Ehrlicher, A. J.; Pappu, R. V. et al. Endocytic proteins with prion-like domains form viscoelastic condensates that enable membrane remodeling. *Proc. Natl. Acad. Sci. U.S.A.* **2021**, *118*, e2113789118.

(26) Lu, T.; Liese, S.; Schoenmakers, L.; Weber, C. A.; Suzuki, H.; Huck, W. T.; Spruijt, E. Endocytosis of coacervates into liposomes. *J. Amer. Chem. Soc.* **2022**, *144*, 13451–13455.

(27) Agudo-Canalejo, J.; Schultz, S. W.; Chino, H.; Migliano, S. M.; Saito, C.; Koyama-Honda, I.; Stenmark, H.; Brech, A.; May, A. I.; Mizushima, N.; Knorr, R. L. Wetting regulates autophagy of phase-separated compartments and the cytosol. *Nature* **2021**, *591*, 142–146.

(28) Ghosh, R.; Satarifard, V.; Lipowsky, R. Different pathways for engulfment and endocytosis of liquid droplets by nanovesicles. *Nat. Comm.* **2023**, *14*, 615.

(29) Lee, Y.; Park, S.; Yuan, F.; Hayden, C. C.; Choi, S. Q.; Stachowiak, J. C. Lateral compression of lipids drives transbilayer coupling of liquid-like protein condensates. *bioRxiv* **2022**, 2022–12.

(30) Paul, S.; Audhya, A.; Cui, Q. Molecular mechanism of GTP binding-and dimerization-induced enhancement of Sar1-mediated membrane remodeling. *Proc. Natl. Acad. Sci. USA* **2023**, *120*, e2212513120.

(31) Kozlov, M. M.; Taraska, J. W. Generation of nanoscopic membrane curvature for membrane trafficking. *Nat. Rev. Mol. Cell Biol.* **2022**, 1–16.

(32) Lipowsky, R.; Döbereiner, H.-G.; Hiergeist, C.; Indrani, V. Membrane curvature induced by polymers and colloids. *Phys. A: Stat. Mech. Appl.* **1998**, *249*, 536–543.

(33) Bremer, A.; Farag, M.; Borcherds, W. M.; Peran, I.; Martin, E. W.; Pappu, R. V.; Mittag, T. Deciphering how naturally occurring sequence features impact the phase behaviours of disordered prion-like domains. *Nat. Chem.* **2022**, *14*, 196–207.

(34) Lin, Y.-H.; Forman-Kay, J. D.; Chan, H. S. Sequence-specific polyampholyte phase separation in membraneless organelles. *Phys. Rev. Lett.* **2016**, *117*, 178101.

(35) Dignon, G. L.; Zheng, W.; Kim, Y. C.; Best, R. B.; Mittal, J. Sequence determinants of protein phase behavior from a coarse-grained model. *PLoS Comput. Biol.* **2018**, *14*, e1005941.

(36) Lin, Y.-H.; Chan, H. S. Phase separation and single-chain compactness of charged disordered proteins are strongly correlated. *Biophys. J.* **2017**, *112*, 2043–2046.

(37) Quiroz, F. G.; Chilkoti, A. Sequence heuristics to encode phase behaviour in intrinsically disordered protein polymers. *Nat. Mater.* **2015**, *14*, 1164–1171.

(38) Schuster, B. S.; Dignon, G. L.; Tang, W. S.; Kelley, F. M.; Ranganath, A. K.; Jahnke, C. N.; Simpkins, A. G.; Regy, R. M.; Hammer, D. A.; Good, M. C.; others Identifying sequence perturbations to an intrinsically disordered protein that determine its phase-separation behavior. *Proc. Natl. Acad. Sci. USA* **2020**, *117*, 11421–11431.

(39) Chatterjee, S.; Maltseva, D.; Kan, Y.; Hosseini, E.; Gonella, G.; Bonn, M.; Parekh, S. H. Lipid-driven condensation and interfacial ordering of FUS. *Sci. Adv.* **2022**, *8*, eabm7528.

(40) Snead, W. T.; Gladfelter, A. S. The Control Centers of Biomolecular Phase Separation: How Membrane Surfaces, PTMs, and Active Processes Regulate Condensation. *Mol. Cell* **2019**, *76*, 295–305.

(41) Chung, J. K.; Huang, W. Y. C.; Carbone, C. B.; Nocka, L. M.; Parikh, A. N.; Vale, R. D.; Groves, J. T. Coupled membrane lipid miscibility and phosphotyrosine-driven protein condensation phase transitions. *Biophys. J.* **2021**, *120*, 1257–1265.

(42) Case, L. B.; M. De Pasquale; Henry, L.; Rosen, M. K. Synergistic phase separation of two pathways promotes integrin clustering and nascent adhesion formation. *eLife* **2022**, *11*, e72588.

(43) Rouches, M.; Veatch, S. L.; Machta, B. B. Surface densities prewet a near-critical membrane. *Proc. Natl. Acad. Sci. USA* **2021**, *118*.

(44) Liu, Z.; Yethiraj, A.; Cui, Q. Sensitive and selective polymer condensation at membrane surface driven by positive co-operativity. *Proc. Natl. Acad. Sci. USA* **2023**, *120*, e2212516120.

(45) Das, R. K.; Pappu, R. V. Conformations of intrinsically disordered proteins are influenced by linear sequence distributions of oppositely charged residues. *Proc. Natl. Acad. Sci. USA* **2013**, *110*, 13392–13397.

(46) Rumyantsev, A. M.; Jackson, N. E.; De Pablo, J. J. Polyelectrolyte complex coacervates: Recent developments and new frontiers. *Annu. Rev. Condens. Matter Phys* **2021**, *12*, 155–176.

(47) Sing, C. E.; Perry, S. L. Recent progress in the science of complex coacervation. *Soft Matter* **2020**, *16*, 2885–2914.

(48) Delaney, K. T.; Fredrickson, G. H. Theory of polyelectrolyte complexation—Complex coacervates are self-coacervates. *J. Chem. Phys.* **2017**, *146*, 224902.

(49) Danielsen, S. P.; McCarty, J.; Shea, J.-E.; Delaney, K. T.; Fredrickson, G. H. Small ion effects on self-coacervation phenomena in block polyampholytes. *J. Chem. Phys.* **2019**, *151*, 034904.

(50) Hazra, M. K.; Levy, Y. Charge pattern affects the structure and dynamics of polyampholyte condensates. *Phys. Chem. Chem. Phys.* **2020**, *22*, 19368–19375.

(51) Melnyk, A.; Namieśnik, J.; Wolska, L. Theory and recent applications of coacervate-based extraction techniques. *Trends Anal. Chem.* **2015**, *71*, 282–292.

(52) Blocher, W. C.; Perry, S. L. Complex coacervate-based materials for biomedicine. *Wiley Interdiscip. Rev. Nanomed. Nanobiotechnol.* **2017**, *9*, e1442.

(53) Wang, Y.; Huang, L.; Shen, Y.; Tang, L.; Sun, R.; Shi, D.; Webster, T. J.; Tu, J.; Sun, C. Electrostatic interactions between polyglutamic acid and polylysine yields stable polyion complex micelles for deoxypodophyllotoxin delivery. *Intl. J. Nanomed.* **2017**, *12*, 7963.

(54) Hwang, J. J.; Stupp, S. I. Poly (amino acid) bioadhesives for tissue repair. *J. Biomater. Sci. Polym. Ed.* **2000**, *11*, 1023–1038.

(55) Richert, L.; Arntz, Y.; Schaaf, P.; Voegel, J.-C.; Picart, C. pH dependent growth of poly (L-lysine)/poly (L-glutamic) acid multilayer films and their cell adhesion properties. *Surf. Sci.* **2004**, *570*, 13–29.

(56) Astoricchio, E.; Alfano, C.; Rajendran, L.; Temussi, P. A.; Pastore, A. The wide world of coacervates: from the sea to neurodegeneration. *Trends in Biochem, Sci.* **2020**, *45*, 706–717.

(57) Shih, L.; Shen, M.-H.; Van, Y.-T. Microbial synthesis of poly (ε-lysine) and its various applications. *Bioresour. Technol.* **2006**, *97*, 1148–1159.

(58) Shen, W.-C. Acid-sensitive dissociation between poly (lysine) and histamine-modified poly (glutamate) as a model for drug-releasing from carriers in endosomes. *Biochim. Biophys. Acta - Gen. Subj.* **1990**, *1034*, 122–124.

(59) Shih, I.-L.; Van, Y.-T.; Shen, M.-H. Biomedical applications of chemically and microbiologically synthesized poly (glutamic acid) and poly (lysine). *Mini. Rev. Med. Chem.* **2004**, *4*, 179–188.

(60) Buescher, J. M.; Margaritis, A. Microbial biosynthesis of polyglutamic acid biopolymer and applications in the biopharmaceutical, biomedical and food industries. *Crit. Rev. Biotechnol.* **2007**, *27*, 1–19.

(61) Van Stevendaal, M. H.; Vasiukas, L.; Yewdall, N. A.; Mason, A. F.; van Hest, J. C. Engineering of biocompatible coacervate-based synthetic cells. *ACS Appl. Mat. Interfaces* **2021**, *13*, 7879–7889.

(62) Wu, H.; Qiao, Y. Engineering coacervate droplets towards the building of multiplex biomimetic protocells. *Supramolec. Mat.* **2022**, 100019.

(63) Priftis, D.; Tirrell, M. Phase behaviour and complex coacervation of aqueous polypeptide solutions. *Soft Matter* **2012**, *8*, 9396–9405.

(64) Tsanai, M.; Frederix, P. W.; Schroer, C. F.; Souza, P. C.; Marrink, S. J. Coacervate formation studied by explicit solvent coarse-grain molecular dynamics with the Martini model. *Chem. Sci.* **2021**, *12*, 8521–8530.

(65) Rumyantsev, A. M.; Jackson, N. E.; Yu, B.; Ting, J. M.; Chen, W.; Tirrell, M. V.; De Pablo, J. J. Controlling complex coacervation via random polyelectrolyte sequences. *ACS Macro Lett.* **2019**, *8*, 1296–1302.

(66) Das, S.; Lin, Y.-H.; Vernon, R. M.; Forman-Kay, J. D.; Chan, H. S. Comparative roles of charge, π, and hydrophobic interactions in sequence-dependent phase separation of intrinsically disordered proteins. *Proc. Natl. Acad. Sci. USA* **2020**, *117*, 28795–28805.

(67) Singh, A. N.; Yethiraj, A. Driving force for the complexation of charged polypeptides. *J. Phys. Chem. B* **2020**, *124*, 1285–1292.

(68) Anila, M. M.; Ghosh, R.; Rozycki, B. Membrane curvature sensing by model biomolecular condensates. *Soft Matter* **2023**, *19*, 3723–3732.

(69) Flory, P. J. Thermodynamics of high polymer solutions. *J. Chem. Phys.* **1942**, *10*, 51–61.

(70) Huggins, M. L. Some properties of solutions of long-chain compounds. *J. Phys. Chem.* **1942**, *46*, 151–158.

(71) Overbeek, J. T. G.; Voorn, M. Phase separation in polyelectrolyte solutions. Theory of complex coacervation. *J. Cell. Comparative Physiol.* **1957**, *49*, 7–26.

(72) Lin, Y.-H.; Song, J.; Forman-Kay, J. D.; Chan, H. S. Random-phase-approximation theory for sequence-dependent, biologically functional liquid-liquid phase separation of intrinsically disordered proteins. *J. Mol. Liq.* **2017**, *228*, 176–193.

(73) Cooke, I. R.; Kremer, K.; Deserno, M. Tunable generic model for fluid bilayer membranes. *Phys. Rev. E* **2005**, *72*, 011506.

(74) Wu, Z.; Cui, Q.; Yethiraj, A. A New Coarse-grained Model for Water: the Importance of Electrostatic Interactions. *J. Phys. Chem. B* **2010**, *114*, 10524–10529.

(75) Samanta, H. S.; Chakraborty, D.; Thirumalai, D. Charge fluctuation effects on the shape of flexible polyampholytes with applications to intrinsically disordered proteins. *J. Chem. Phys.* **2018**, *149*, 163323.

(76) Souza, P. C.; Alessandri, R.; Barnoud, J.; Thallmair, S.; Faustino, I.; Grünewald, F.; Patmanidis, I.; Abdizadeh, H.; Bruininks, B. M.; Wassenaar, T. A.; others Martini 3: a general purpose force field for coarse-grained molecular dynamics. *Nat. Method* **2021**, *18*, 382–388.

(77) Ando, D.; Zandi, R.; Kim, Y. W.; Colvin, M.; Rexach, M.; Gopinathan, A. Nuclear pore complex protein sequences determine overall copolymer brush structure and function. *Biophys. J.* **2014**, *106*, 1997–2007.

(78) Roberts, S.; Harmon, T. S.; Schaal, J. L.; Miao, V.; Li, K. J.; Hunt, A.; Wen, Y.; Oas, T. G.; Collier, J. H.; Pappu, R. V.; others Injectable tissue integrating networks from recombinant polypeptides with tunable order. *Nat. Mater.* **2018**, *17*, 1154–1163.

(79) Latham, A. P.; Zhang, B. Maximum entropy optimized force field for intrinsically disordered proteins. *J. Chem. Theo. Comp.* **2019**, *16*, 773–781.

(80) Nguemaha, V.; Zhou, H.-X. Liquid-liquid phase separation of patchy particles illuminates diverse effects of regulatory components on protein droplet formation. *Sci. Rep.* **2018**, *8*, 1–11.

(81) Feric, M.; Vaidya, N.; Harmon, T. S.; Mitrea, D. M.; Zhu, L.; Richardson, T. M.; Kriwacki, R. W.; Pappu, R. V.; Brangwynne, C. P. Coexisting liquid phases underlie nucleolar subcompartments. *Cell* **2016**, *165*, 1686–1697.

(82) Thomasen, F. E.; Pesce, F.; Roesgaard, M. A.; Tesei, G.; Lindorff-Larsen, K. Improving Martini 3 for disordered and multidomain proteins. *J. Chem. Theo. Comp.* **2022**, *18*, 2033–2041.

(83) Benayad, Z.; von Bulow, S.; Stelzl, L. S.; Hummer, G. Simulation of FUS protein condensates with an adapted coarse-grained model. *J. Chem. Theo. Comp.* **2021**, *17*, 525–537.

(84) Gruijs da Silva, L. A.; Simonetti, F.; Hutten, S.; Riemenschneider, H.; Sternburg, E. L.; Pietrek, L. M.; Gebel, J.; Dötsch, V.; Edbauer, D.; Hummer, G. et al. Disease-linked TDP-43 hyperphosphorylation suppresses TDP-43 condensation and aggregation. *The EMBO Journal* **2022**, *n/a*, e108443.

(85) Marrink, S. J.; Tieleman, D. P. Perspective on the Martini model. *Chem. Soc. Rev.* **2013**, *42*, 6801–6822.

(86) Eid, J.; Razmazma, H.; Jraij, A.; Ebrahimi, A.; Monticelli, L. On calculating the bending modulus of lipid bilayer membranes from buckling simulations. *J. Phys. Chem. B* **2020**, *124*, 6299–6311.

(87) DeLano, W. L.; others Pymol: An open-source molecular graphics tool. *CCP4 Newsl. Prot. Crystallogr.* **2002**, *40*, 82–92.

(88) Bussi, G.; Donadio, D.; Parrinello, M. Canonical sampling through velocity rescaling. *J. Chem. Phys.* **2007**, *126*, 014101.

(89) Parrinello, M.; Rahman, A. Polymorphic transitions in single crystals: A new molecular dynamics method. *J. Appl. Phys.* **1981**, *52*, 7182–7190.

(90) Berendsen, H. J.; Postma, J. v.; Van Gunsteren, W. F.; DiNola, A.; Haak, J. R. Molecular dynamics with coupling to an external bath. *J. Chem. Phys.* **1984**, *81*, 3684–3690.

(91) Abraham, M. J.; Murtola, T.; Schulz, R.; Páll, S.; Smith, J. C.; Hess, B.; Lindahl, E. GROMACS: High performance molecular simulations through multi-level parallelism from laptops to supercomputers. *SoftwareX* **2015**, *1*, 19–25.

(92) Tribello, G. A.; Bonomi, M.; Branduardi, D.; Camilloni, C.; Bussi, G. PLUMED 2: New feathers for an old bird. *Comp. Phys. Comm.* **2014**, *185*, 604–613.

(93) Humphrey, W.; Dalke, A.; Schulten, K. VMD: visual molecular dynamics. *J. Mol. Graph.* **1996**, *14*, 33–38.

(94) Sawle, L.; Ghosh, K. A theoretical method to compute sequence dependent configurational properties in charged polymers and proteins. *J. Chem. Phys.* **2015**, *143*, 08B615_1.

(95) May, S.; Harries, D.; Ben-Shaul, A. Lipid demixing and protein-protein interactions in the adsorption of charged proteins on mixed membranes. *Biophys. J.* **2000**, *79*, 1747–1760.

(96) Heimburg, T.; Angerstein, B.; Marsh, D. Binding of peripheral proteins to mixed lipid membranes: effect of lipid demixing upon binding. *Biophys. J.* **1999**, *76*, 2575–2586.

(97) Das, M.; Dahal, U.; Mesele, O.; Liang, D.; Cui, Q. Molecular dynamics simulation of interaction between functionalized nanoparticles with lipid membranes: Analysis of coarse-grained models. *J. Phys. Chem. B* **2019**, *123*, 10547–10561.

(98) Stumpf, B. H.; Nowakowski, P.; Eggeling, C.; Maciołek, A.; Smith, A.-S. Protein induced lipid demixing in homogeneous membranes. *Phys. Rev. Research* **2021**, *3*, L042013.

(99) Jarsch, I. K.; Daste, F.; Gallop, J. L. Membrane curvature in cell biology: An integration of molecular mechanisms. *J. Cell. Biol.* **2016**, *214*, 375–387.

(100) Mandal, T.; Spagnolie, S. E.; Audhya, A.; Cui, Q. Protein-induced membrane curvature in coarse-grained simulations. *Biophys. J.* **2021**, *120*, 3211–3221.

(101) Alimohamadi, H.; Rangamani, P. Modeling membrane curvature generation due to membrane–protein interactions. *Biomolecules* **2018**, *8*, 120.

(102) McMahon, H. T.; Boucrot, E. Membrane curvature at a glance. *J. Cell Sci.* **2015**, *128*, 1065–1070.

(103) Baumgart, T.; Capraro, B. R.; Zhu, C.; Das, S. L. Thermodynamics and mechanics of membrane curvature generation and sensing by proteins and lipids. *Annu. Rev. Phys. Chem.* **2011**, *62*, 483–506.

(104) Kim, Y. W.; Sung, W. Membrane curvature induced by polymer adsorption. *Phys. Rev. E* **2001**, *63*, 041910.

(105) Hiergeist, C.; Indrani, V.; ; Lipowsky, R. Membranes with anchored polymers at the adsorption transition. *Europhys. Lett.* **1996**, *36*, 491.

(106) Mondal, S.; Cui, Q. Coacervation induced remodeling of nanovesicles. *J. Phys. Chem. Lett.* **2023**, *14*, 4532–4540.

(107) Dickey, A.; Faller, R. Examining the contributions of lipid shape and headgroup charge on bilayer behavior. *Biophys. J.* **2008**, *95*, 2636–2646.

(108) Campelo, F.; McMahon, H. T.; Kozlov, M. M. The hydrophobic insertion mechanism of membrane curvature generation by proteins. *Biophys. J.* **2008**, *95*, 2325–2339.

(109) Zimmerberg, J.; Kozlov, M. M. How proteins produce cellular membrane curvature. *Nat. Rev. Mol. Cell Biol.* **2006**, *7*, 9–19.

(110) Lee, M. C.; Orci, L.; Hamamoto, S.; Futai, E.; Ravazzola, M.; Schekman, R. Sar1p N-terminal helix initiates membrane curvature and completes the fission of a COPII vesicle. *Cell* **2005**, *122*, 605–617.

(111) Stachowiak, J. C.; Schmid, E. M.; Ryan, C. J.; Ann, H. S.; Sasaki, D. Y.; Sherman, M. B.; Geissler, P. L.; Fletcher, D. A.; Hayden, C. C. Membrane bending by protein–protein crowding. *Nat. Cell Biol.* **2012**, *14*, 944–949.

(112) Busch, D. J.; Houser, J. R.; Hayden, C. C.; Sherman, M. B.; Lafer, E. M.; Stachowiak, J. C. Intrinsically disordered proteins drive membrane curvature. *Nat. Comm.* **2015**, *6*, 1–11.

(113) Liese, S.; Carlson, A. Membrane shape remodeling by protein crowding. *Biophys. J.* **2021**, *120*, 2482–2489.

(114) Jarin, Z.; Newhouse, J.; Voth, G. A. Coarse-grained force fields from the perspective of statistical mechanics: Better understanding of the origins of a MARTINI hangover. *J. Chem. Theo. Comp.* **2021**, *17*, 1170–1180.

(115) Wu, Z.; Cui, Q.; Yethiraj, A. Driving force for the association of hydrophobic peptides: the importance of electrostatic interactions in coarse-grained water models. *J. Phys. Chem. Lett.* **2011**, *2*, 1794–1798.

(116) Vivcharuk, V.; Kaznessis, Y. Free Energy Profile of the Interaction between a Monomer or a Dimer of Protegrin-1 in a Specific Binding Orientation and a Model Lipid Bilayer. *J. Phys. Chem. B* **2010**, *114*, 2790–2797.

(117) Chowdhury, A.; Borgia, A.; Ghosh, S.; Sottini, A.; Mitra, S.; Eapen, R. S.; Borgia, M. B.; Yang, T.; Galvanetto, N.; Ivanovic, M. T. et al. Driving forces of the complex formation between highly charged disordered proteins. *Proc. Natl. Acad. Sci. USA* **2023**, *120*, e2304036120.

(118) Mukherjee, S.; Schäfer, L. V. Thermodynamic forces from protein and water govern condensate formation of an intrinsically disordered protein domain. *Nat. Comm.* **2023**, *14*, 5892.

(119) Fuhrmans, M.; Sanders, B. P.; Marrink, S.-J.; de Vries, A. H. Effects of bundling on the properties of the SPC water model. *Theo. Chem. Acc.* **2010**, *125*, 335–344.

(120) Choi, E.; Mondal, J.; Yethiraj, A. Coarse-grained models for aqueous polyethylene glycol solutions. *J. Phys. Chem. B* **2014**, *118*, 323–329.

(121) Schuh, A. L.; Audhya, A. The ESCRT machinery: From the plasma membrane to endosomes and back again. *Crit. Rev. Biochem. Mol. Biol.* **2014**, *49*, 242–261.

(122) Towns, J.; Cockerill, T.; Dahan, M.; Foster, I.; Gaither, K.; Grimshaw, A.; Hazelwood, V.; Lathrop, S.; Lifka, D.; Peterson, G. D. et al. XSEDE: Accelerating Scientific Discovery. *Comput Sci. & Engn.* **2014**, *16*, 62–74.

TOC Graphic

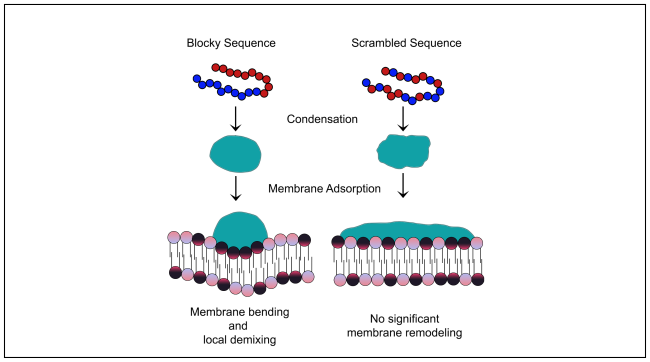
Blocky Sequence
Scrambled Sequence
Condensation
Membrane Adsorption
Membrane bending
and
local demixing
No significant
membrane remodeling